MATERIALS CHEMISTRY FRONTIERS

RESEARCH ARTICLE

View Article Online
View Journal | View Issue

Cite this: *Mater. Chem. Front.*, 2022, **6**, 3442

Thermally activated delayed fluorescence dendrimers achieving 20% external quantum efficiency for solution-processed OLEDs†

Cheng Zhang,‡[a] Hao Yan,‡[b] Yuting He,‡[c] Yongshuai Chai*[d] and Deyun Zhou*[c]

Two multi-carbazole-encapsulated TADF dendrimers were obtained by coupling tercarbazole (*t*BuTCz or MeOTCz) and di(pyridin-3-yl)methanone (DPyM) units. Both **tBuTCz-DPyM** and **MeOTCz-DPyM** show small singlet–triplet energy gap (ΔE_{ST}) values (0.01 *vs.* 0.02 eV) and high photoluminescence quantum yield (PLQY) values (66.2 *vs.* 55.0%). High-performance solution-processed OLEDs based on ***t*BuTCz-DPyM** and **MeOTCz-DPyM** as the emissive layer were fabricated. The ***t*BuTCz-DPyM**-based solution-processed device exhibited a maximum current efficiency (CE_{max}) of 52.6 cd A^{-1}, a maximum external quantum efficiency (EQE_{max}) of 20.4% and a maximum luminance (L_{max}) of 6165 cd m^{-2} with a low turn-on voltage of 3.2 V. The **MeOTCz-DPyM**-based solution-processed device also showed an efficient performance with a CE_{max} of 27.0 cd A^{-1}, an EQE_{max} of 9.2%, an L_{max} of 8169 cd m^{-2} and a low turn-on voltage of 3.4 V. The ***t*BuTCz-DPyM**-based device (I) and the **MeOTCz-DPyM**-based device (II) show Commission internationale de l'éclairage (CIE) coordinates of (0.25, 0.48) and (0.37, 0.54), respectively. Both ***t*BuTCz-DPyM** and **MeOTCz-DPyM** demonstrate a high performance among solution-processed OLEDs with TADF dendrimers.

Received 17th August 2022,
Accepted 27th September 2022

DOI: 10.1039/d2qm00833e

rsc.li/frontiers-materials

1. Introduction

Due to their wide viewing angle, high response speed, high brightness and lightweight properties, organic light-emitting diodes (OLEDs) had been developed as commercial technologies for next-generation displays and lighting.[1–5] Generally, the fabrication of OLEDs can be divided into vacuum-deposited and solution-processed devices. The construction of multiple organic functional layers for vacuum-deposited OLEDs has been proved to be efficient.[6–8] However, due to the limited deposited space, low material utilization and high manufacturing costs, the development of vacuum-deposited OLEDs has been restricted. Therefore, it is more important to develop solution-processed OLEDs. At this stage, great progress has been made with solution-processed OLEDs.[9–16] Nonetheless, the performance of solution-processed OLEDs still needs to be greatly improved, and comparison with that of vacuum-deposited OLEDs is difficult. In recent years, as a third-generation light-emitting material in OLEDs, based on their advantages of being heavy metal-free, low cost and achieving a 100% internal quantum efficiency (IQE) through efficient reverse intersystem crossing (RISC) procedures, thermally activated delayed fluorescence (TADF) emitters have received great attention.[17–22] Thus, it is particularly important to develop high-performance solution-processed TADF materials.

Small-molecule TADF emitters have the disadvantages of being low-molecular-weight compounds, with poor solution-processability and a high crystallization tendency, which are not suitable for solution-processed OLEDs.[23,24] In recent years, polymers and dendritic TADF molecules have been widely developed as solution-processed OLED materials.[25–30] In particular, due to their definite structural composition, good film-forming properties and high purity, dendrimers are a type of ideal solution-processing OLED material.[31–34] Because multi-carbazole-encapsulated molecules have good solubility, a good hole-transport capacity, amorphous film-forming properties and good thermal stability, these are suit for solution-processed OLEDs. Therefore, a suitable design strategy for multi-carbazole-encapsulated

[a] *Key Laboratory of Functional Textile Material and Product (Ministry of Education), School of Textile Science and Engineering, Xi'an Polytechnic University, Xi'an, Shaanxi, 710048, P. R. China*
[b] *School of Advanced Materials, Peking University Shenzhen Graduate School, Peking University, Shenzhen, 518055, P. R. China*
[c] *School of Microelectronics, Northwestern Polytechnical University, Xi'an, Shaanxi, 710129, P. R. China. E-mail: dyzhou@nwpu.edu.cn*
[d] *Interdisciplinary Research Center on Biology and Chemistry, Shanghai Institute of Organic Chemistry, Chinese Academy of Sciences, Shanghai, 201210, P. R. China. E-mail: Chaiys@sioc.ac.cn*

† Electronic supplementary information (ESI) available. See DOI: https://doi.org/10.1039/d2qm00833e

‡ These authors contributed equally to this work.

molecules for the construction of TADF dendrimers could be beneficial for solution-processed OLEDs.[35–39] In this paper, we report two TADF dendrimers with multi-carbazole encapsulation, named ***t*BuTCz-DPyM** and **MeOTCz-DPyM**, which comprise di(pyridin-3-yl)methanone (DPyM) as the acceptor core coupled with 3,3″,6,6″-tetra-*tert*-butyl-9′*H*-9,3′:6′,9″-tercarbazole (*t*BuTCz) or 3,3″,6,6″-tetramethoxy-9′*H*-9,3′:6′,9″-tercarbazole (MeOTCz) as the donor units. The solution-processed devices based on ***t*BuTCz-DPyM** and **MeOTCz-DPyM** as the doped emissive layer show a high performance with maximum current efficiency (CE_{max}) values of 52.6 and 27.0 cd A^{-1}, maximum external quantum efficiency (EQE_{max}) values of 20.4 and 9.2%, maximum luminance (L_{max}) values of 6165 and 8169 cd m^{-2} at 8 V, and low turn-on voltages of 3.2 and 3.4 V, respectively. In addition, the full-width at half-maximum (FWHM) of the EL spectrum for ***t*BuTCz-DPyM** is narrow, at 84 nm.

2. Results and discussion

2.1. Synthesis and structural characterization

As shown in Scheme S1 (ESI†), the target compounds for ***t*BuTCz-DPyM** and **MeOTCz-DPyM** were prepared *via* the Ullmann C–N coupling reaction of DPyM with *t*BuTCz or MeOTCz, respectively.[40,41] The chemical structures of the two dendrimers were confirmed using ^{1}H NMR and ^{13}C NMR and high-resolution MS.

2.2. Thermal properties and film-forming properties

The two materials showed good thermal stability, which was indicated by their high decomposition temperature (T_d, corresponding to 5% weight loss) values of 443 and 446 °C for ***t*BuTCz-DPyM** and **MeOTCz-DPyM**, respectively, and the glass transition temperature (T_g) for ***t*BuTCz-DPyM** and **MeOTCz-DPyM** reached 260 and 268 °C, respectively (Fig. S1, ESI†). Moreover, in order to evaluate the morphological stability of the target compounds, atomic force microscopy (AFM) was utilized to explore the surface images of their neat films. As shown in Fig. S2 (ESI†), the surfaces of the two films were smooth and pinhole-free, and the root-mean-square (RMS) roughness was 0.44 nm and 0.46 nm for ***t*BuTCz-DPyM** and **MeOTCz-DPyM**, respectively. Therefore, the two emitters can provide uniform amorphous films for solution-processed devices, and the introduction of the *tert*-butyl group into the molecule provides better film-forming properties than for the methoxy-containing emitter.

2.3. Electrochemical and computational properties

The electrochemical behavior of the dendrimers was investigated using cyclic voltammetry (CV). As shown in Fig. S3 (ESI†), both of the compounds displayed one oxidation wave. According to the onset potentials, the highest occupied molecular orbital (HOMO) energy levels of ***t*BuTCz-DPyM** and **MeOTCz-DPyM** were estimated to be −5.47 and −5.12 eV, respectively. According to the optical bandgaps, the lowest unoccupied molecular orbital (LUMO) energy levels of ***t*BuTCz-DPyM** and **MeOTCz-DPyM** were calculated to be −2.70 eV and −2.52 eV, respectively. To gain insight into the electronic nature and geometry of the emitters, density functional theory (DFT) calculations were performed at the B3LYP/6-31G* level. As shown in Fig. 1, the HOMO and LUMO of the two compounds were located on the electron-donating multi-carbazole unit and the electron-withdrawing dipyridyl ketone unit, respectively. It was shown that the two molecules have a small HOMO–LUMO overlap, which indicates strong charge-transfer (CT) character and a small electron-exchange energy.[42,43] The calculated HOMO levels of ***t*BuTCz-DPyM** and **MeOTCz-DPyM** were −5.17 and −4.88 eV, while the calculated LUMO levels were −2.41 and −2.40 eV, respectively. Due to the stronger electron-donating ability of the methoxy group over the *tert*-butyl group, the HOMO level of **MeOTCz-DPyM** is shallower than that of ***t*BuTCz-DPyM**.[16] This matches the experimental values obtained from the CV curves.

2.4. Photophysical properties

The two materials displayed similar absorption spectra. The weak absorption bands in the range of 320–450 nm assigned to the CT transitions from the *t*BuTCz or MeOTCz as donor units to DPyM as the acceptor unit. The ***t*BuTCz-DPyM** and **MeOTCz-DPyM** materials showed emission peaks at 521 and 554 nm in solution, respectively. Fig. 2b shows the fluorescence and phosphorescence spectra of the two compounds in their film states. According to the onsets of the fluorescence and phosphorescence spectra, ΔE_{ST} was calculated to be 0.01 eV for ***t*BuTCz-DPyM**, and 0.02 eV for **MeOTCz-DPyM**. The small ΔE_{ST} values indicated that an up-conversion process of the triplet excitons into their singlet state could occur efficiently through RISC, which results in the TADF phenomenon.[42,43] The corresponding data are summarized in Table 1.

Moreover, the two dendrimers also showed small calculated ΔE_{ST} values of 0.07 and 0.03 eV for ***t*BuTCz-DPyM** and **MeOTCz-DPyM**, respectively. The dendrimers of ***t*BuTCz-DPyM** and **MeOTCz-DPyM** have a high PLQY in the films of 63.5 and 55.0%, respectively, which indicated that, compared with **MeOTCz-DPyM** with methoxy groups, ***t*BuTCz-DPyM** with *tert*-butyl groups can better reduce the concentration quenching caused by molecular aggregation. As shown in Fig. 3, transient PL measurements were carried out to prove the TADF features of the two dendrimers in the film state at room temperature. Both target compounds showed a multi-exponential decay with a short lifetime of 7.0 ns and a long lifetime of 9.5 μs for ***t*BuTCz-DPyM**, and a short lifetime of 15.7 ns and a long lifetime of 7.9 μs for **MeOTCz-DPyM**, which is attributed to TADF.[36] In order to gain a deeper insight into the RISC process, the rate constants of the two materials were calculated using reported methods.[44] As shown in Table S1 (ESI†), the rate constant for radiative decay from the S_1 state ($k_{r,s}$) of ***t*BuTCz-DPyM** and **MeOTCz-DPyM** was calculated to be 5.0×10^7 and 1.9×10^7 s^{-1}, respectively. This is equivalent to the value of conventional fluorescent materials. Moreover, the rate constant of non-radiative decay from the S_1 state ($k_{nr,S}$) of ***t*BuTCz-DPyM** and **MeOTCz-DPyM** was estimated to be 2.9×10^7

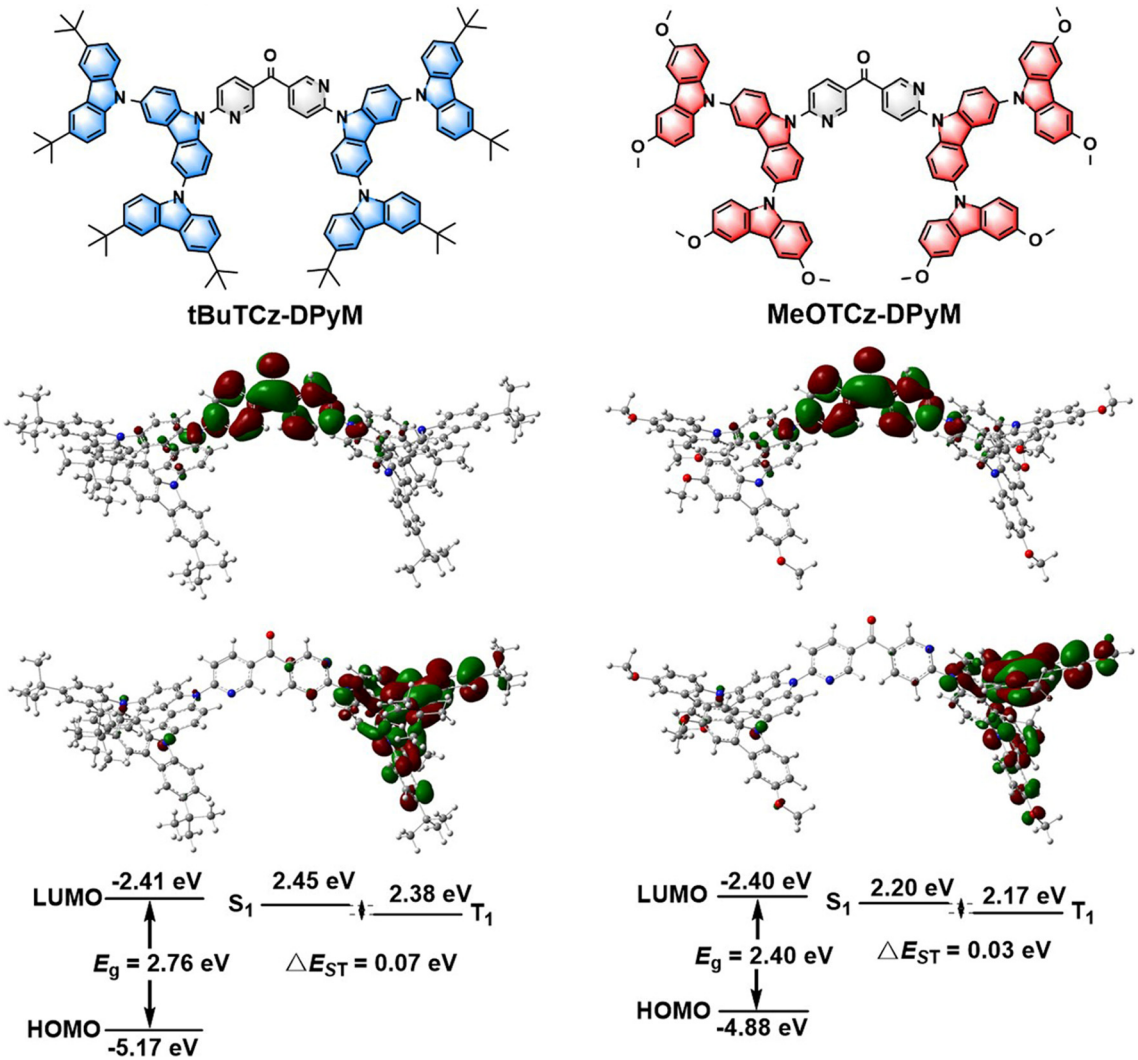

Fig. 1 Chemical structures (top), B3LYP/6-31G*-optimized molecular orbitals for the HOMO (lower middle) and LUMO (upper middle), and the energy levels (bottom) of the ***t*BuTCz-DPyM** (left) and **MeOTCz-DPyM** (right) emitters.

and 1.6×10^7 s^{-1}, respectively. The ratio of $k_{r,\,S}$ to $k_{nr,S}$ is 1.7 for ***t*BuTCz-DPyM** and 1.2 for **MeOTCz-DPyM**. Therefore, the ratio of $k_{r,\,S}$ to $k_{nr,S}$ for ***t*BuTCz-DPyM** is slightly higher than that of **MeOTCz-DPyM**, which leads to a slightly higher PLQY value for ***t*BuTCz-DPyM** compared with **MeOTCz-DPyM**.[45] Furthermore, the k_{RISC} values of the two emitters were relatively fast, with the corresponding values of 1.8×10^5 s^{-1} for ***t*BuTCz-DPyM** and 2.4×10^5 s^{-1} for **MeOTCz-DPyM**, which exhibited an effective RISC process, leading to small ΔE_{ST} values.

2.5. Electroluminescent properties

As shown in Fig. 4, the relative energy-level alignments, the electroluminescence (EL) spectra, current density–voltage–luminance (*J*–*V*–*L*) characteristics, and the external quantum efficiency–current density curves of the optimized devices are displayed, and the corresponding parameters are summarized in Table 2. Both of the solution-processed devices were fabricated with the following structures: ITO/PEDOT:PSS (40 nm)/PVK (5 nm)/mCBP: emitter (8 wt%, 60 nm)/TPBI (40 nm)/Yb (5 nm)/Ag (120 nm). PEDOT:PSS is poly(3,4-ethylenedioxythiophene):poly(styrenesulfonic acid), which act as the hole-injection layer; PVK is poly(*N*-vinylcarbazole), which acts as the hole-transporting layer; and TPBI is 1,3,5-tris(*N*-phenylbenzimiazole-2-yl)benzene, which serves as the electron-transporting layer. The EQE–current density curves show CE_{max} = 52.6 cd A^{-1}, and EQE_{max} = 20.4% for the ***t*BuTCz-DPyM**-based device (device I), and CE_{max} = 27.0 cd A^{-1}, and EQE_{max} = 9.2% for the **MeOTCz-DPyM**-based device (device II). In addition, the full-width at half-maximum (FWHM) of the EL spectrum of device I is only 84 nm, narrower than that of device II (115 nm), and the EL spectrum for devices I and II exhibits, respectively, bluish-green and green emission with a maximum at 503 and 530 nm and Commission internationale de l'éclairage (CIE) coordinates of (0.25, 0.48) and (0.37, 0.54). Both emitters have small ΔE_{ST} and high PLQY values, which can not only ensure an effective RISC process but also provide high-efficiency emission. Hence, both materials could be used to obtain high-performance devices.[37] Moreover, because the

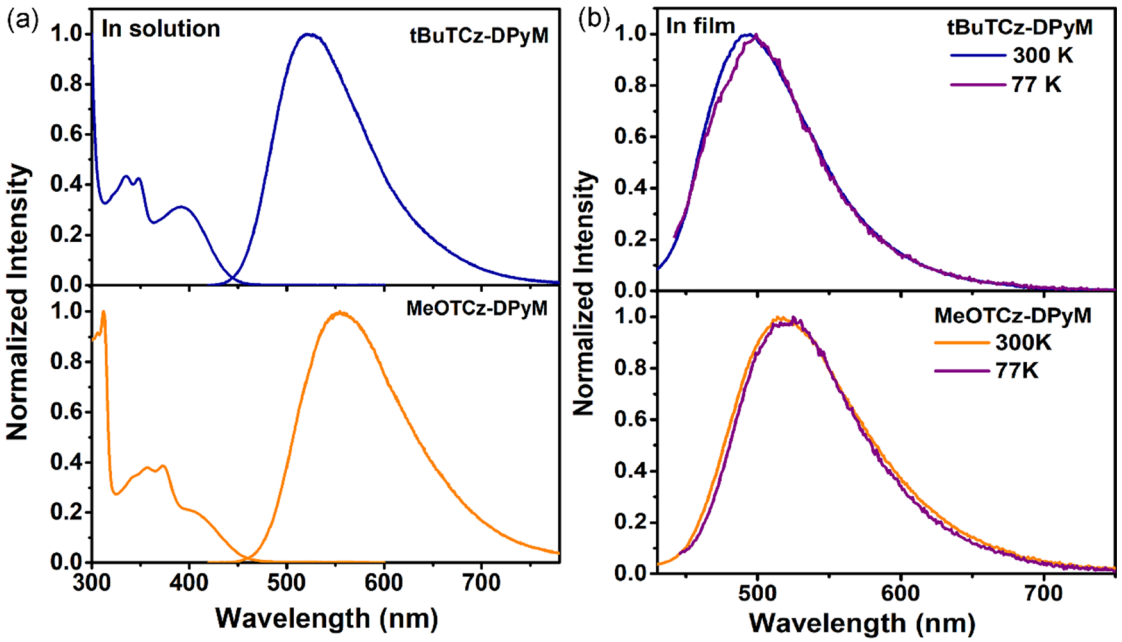

Fig. 2 UV-Vis absorption and PL spectra of ***t*BuTCz-DPyM** and **MeOTCz-DPyM** in (a) dilute toluene solution, and (b) the film state (8 wt% doped in mCBP). Fluorescence spectra at room temperature (300 K) and phosphorescence spectra at 77 K for ***t*BuTCz-DPyM** and **MeOTCz-DPyM** in doped films (8 wt% doped in mCBP).

Table 1 Photophysical, electrochemical and thermal stability data of ***t*BuTCz-DPyM** and **MeOTCz-DPyM**

Compound	λ_{abs}[a] (nm)	λ_{PL}[a]/λ_{PL}[b] (nm)	Φ_{PL}[b] (%)	HOMO[c]/HOMO[d] (eV)	LUMO[e]/LUMO[d] (eV)	ΔE_{ST}[f]/ΔE_{ST}[d] (eV)	k_{RISC}[g] (s^{-1})	τ_p/τ_d[h] [ns]/[μs]	T_d/T_g[i] (°C)
***t*BuTCz-DPyM**	392	521/495	63.5	−5.47/−5.17	−2.70/−2.41	0.01/0.07	1.8×10^5	7.0/9.5	443/260
MeOTCz-DPyM	405	554/514	55.0	−5.12/−4.88	−2.52/−2.40	0.02/0.03	2.4×10^5	15.7/7.9	446/268

[a] Measured in toluene solution. [b] Measured in the film state. [c] HOMO energy levels deduced from the equation HOMO = $-(4.8 + E_{ons}^{ox})$. [d] Obtained from quantum calculations using B3LYP/6-31G*. [e] LUMO energy levels obtained from the equation LUMO = HOMO + E_{opt}^{g}. [f] Estimated from the onset of fluorescence spectrum at 300 K and phosphorescence spectrum at 77 K. [g] k_{RISC}: the rate constant for RISC from the triplet excited state to the singlet excited state. [h] Measured in thin films on a quartz substrate at 300 K. [i] Measured *via* TGA/DSC at a heating rate of 10 °C min^{-1}.

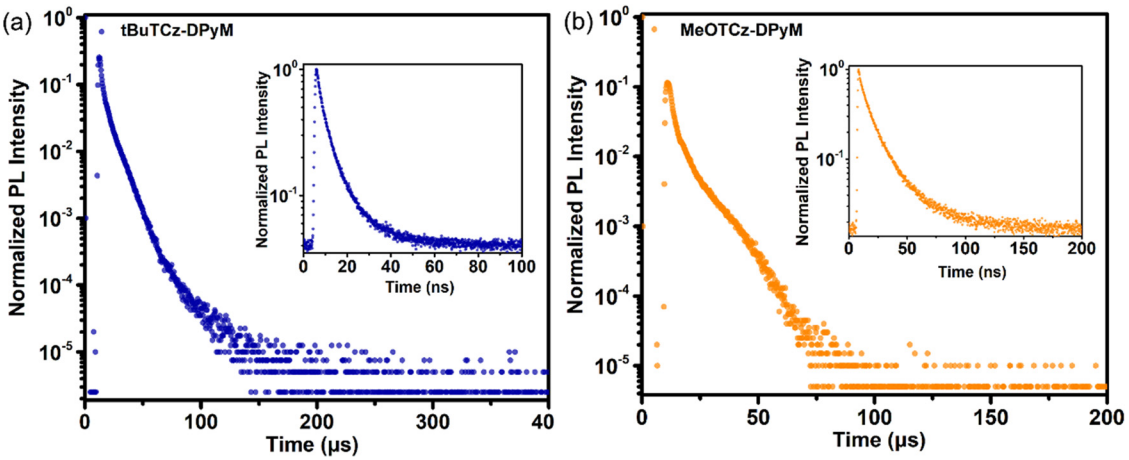

Fig. 3 Transient decay curves of ***t*BuTCz-DPyM** (a) and **MeOTCz-DPyM** (b) in doped films (8 wt% doped in mCBP) at 300 K. Inset: prompt fluorescence.

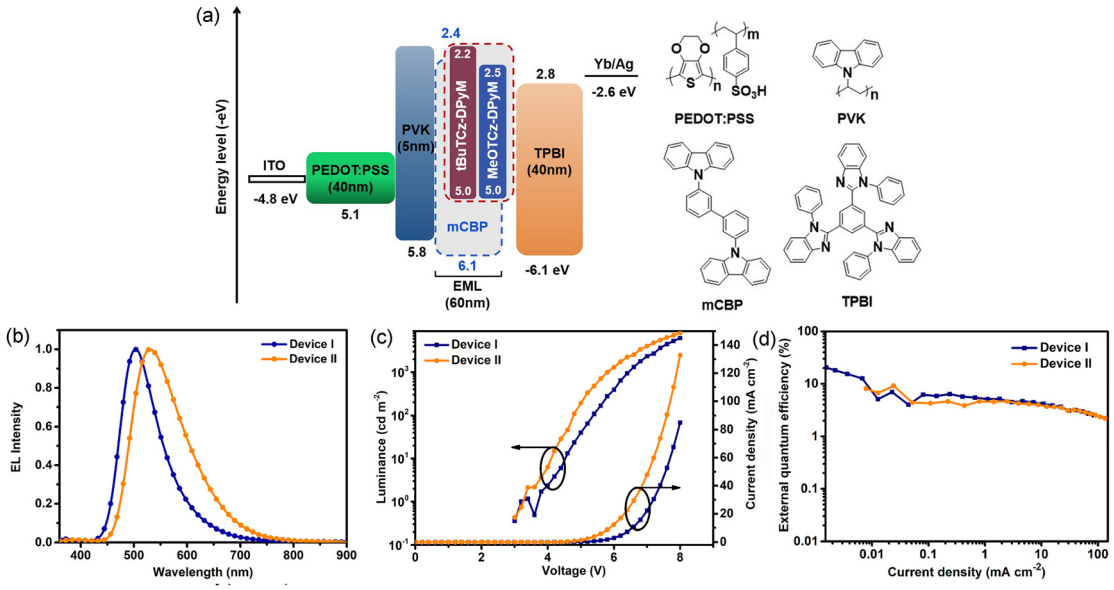

Fig. 4 (a) Relative energy-level alignment of the devices (left) and chemical structures of the materials (right); (b) EL spectra of the devices; (c) current density–voltage–luminance (*J*–*V*–*L*) characteristics of the devices; and (d) external quantum efficiency–current density characteristics of the devices.

Table 2 EL characteristics of devices I and II

Device	λ_{ELmax}[a] (nm)	FWHM (nm)	V_{on}[b] (V)	L_{max}[c] (cd m^{-2})	CE_{max}[d] (cd A^{-1})	EQE_{max}[e] (%)	CIE[f] (*x*, *y*)
I	503	84	3.2	6165	52.6	20.4	0.25, 0.48
II	530	115	3.4	8169	27.0	9.2	0.37, 0.54

[a] EL emission peak. [b] Turn-on voltage recorded at 1 cd m^{-2}. [c] Maximum luminance at 8 V. [d] The maximum current efficiency. [e] The maximum external quantum efficiency. [f] Commission internationale de l'éclairage coordinates.

tert-butyl group has good solubility and electrochemical stability, the ***t*BuTCz-DPyM** emitter, which contains *tert*-butyl groups, is more suitable for solution-processed OLEDs than **MeOTCz-DPyM**, which will lead to a better performance.[38,39]

3. Conclusions

In conclusion, we have developed two new TADF dendrimers based on tercarbazole as the donor and di(pyridin-3-yl)methanone as the accepter. Both ***t*BuTCz-DPyM** and **MeOTCz-DPyM** have excellent thermal stability, good film-forming properties, a small ΔE_{ST} value, and a relatively high PLQY. Two solution-processed devices based on ***t*BuTCz-DPyM** and **MeOTCz-DPyM** as the emitter showed relatively high values, respectively, for CE_{max} of 52.6 and 27.0 cd A^{-1}, EQE_{max} of 20.4% and 9.2%, L_{max} of 6165 and 8169 cd m^{-2} at 8 V, and with low a turn-on voltage of 3.2 and 3.4 V. In particular, the ***t*BuTCz-DPyM**-based solution-processed device showed a bluish-green emission with CIE coordinates of (0.25, 0.48), which possess a narrow FWHM of 84 nm. By contrast, the **MeOTCz-DPyM**-based solution-processed device showed a green emission with CIE coordinates of (0.37, 0.54). These are high efficiencies among solution-processed TADF dendrimer OLEDs. High-performance, solution-processable TADF dendrimers have been developed that are beneficial for the practical application of large-area manufacturing based on solution processing.

4. Experimental section

4.1. General information

Unless otherwise stated, all commercial chemicals are used directly without further purification. All solvents are analytical grade and freshly distilled before use. Anhydrous toluene was refluxed with sodium and anhydrous dichloromethane was refluxed with calcium hydride, followed by fresh distillation before use. ^{1}H NMR and ^{13}C NMR spectra were recorded in $CDCl_3$ with tetramethylsilane (TMS) as the internal standard using a Bruker Avance 600 MHz spectrometer. HRMS (Q-TOF) spectra were obtained using an Impact II spectrometer (Bruker Daltonics Inc.). UV-Vis absorption spectra were collected using a Mapada UV-1800PC recording spectrophotometer. Photoluminescence (PL) spectra were recorded using a PerkinElmer LS-55 fluorescence spectrophotometer. The absolute PLQY values of the emitters in the solid state were measured using an Edinburgh FLS 980 spectrophotometer with an integrating sphere under ambient conditions. TGA was carried out using a Hitachi STA7300 instrument at a heating rate of 10 °C min^{-1} under a nitrogen atmosphere. DSC was carried out using a Mettler Toledo (DSC1) instrument at a heating rate of 10 °C min^{-1} under a nitrogen flow. CV was measured at room temperature using a CorrTest electrochemical workstation. The CV system was constructed using a platinum plate as the working electrode, a platinum wire as the auxiliary electrode and $Ag/AgNO_3$ (0.1 mol L^{-1} in acetonitrile) as the quasi-reference

electrode with ferrocenium/ferrocene (Fc^+/Fc) as the external standard. Tetrabutylammonium perchlorate (0.1 M) was used as the supporting electrolyte.

The synthesis of *t*BuTCz, MeOTCz and DPyM was completed according to the reference methods.[36,40,46]

Synthesis of *t*BuTCz-DPyM. *t*BuTCz (346 mg, 0.48 mmol), DPyM (80 mg, 0.23 mmol), CuI (9.2 mg, 0.05 mmol), K_3PO_4 (1.0 g, 4.8 mmol) and 1,2-diaminocyclohexane (8.0 mg, 0.07 mmol) were added to the system, which was then purged with argon 3 times. The dioxane (4 ml) was added to the system. The reaction was stirred at 110 °C for 12 h. After the reaction, the mixture was filtered using a filter paper. The crude product was obtained after removing the solvent, and was purified *via* column chromatography (silica, hexane/ethyl acetate, v/v 5 : 1) to afford the ***t*BuTCz-DPyM** compound as a yellow solid with a yield of 52%. ^{1}H NMR (600 MHz, $CDCl_3$) δ 9.38 (d, J = 1.8 Hz, 2H), 8.64 (dd, J = 8.4, 1.8 Hz, 2H), 8.33 (d, J = 8.4 Hz, 4H), 8.26 (s, 4H), 8.17 (s, 8H), 8.10 (d, J = 8.4 Hz, 2H), 7.74 (dd, J = 9.0, 1.8 Hz, 4H), 7.48 (d, J = 9.6 Hz, 8H), 7.38 (d, J = 9.0 Hz, 8H), 1.47 (s, 72H). ^{13}C NMR (150 MHz, $CDCl_3$) δ 190.65, 154.78, 151.55, 142.81, 140.12, 139.83, 138.33, 132.83, 129.69, 126.36, 125.89, 123.67, 123.26, 119.13, 117.76, 116.30, 113.36, 109.03, 34.75, 32.03, 29.71. HRMS (APCI) m/z: $[M + H]^+$ calcd for $C_{115}H_{115}N_8O^+$, 1623.9188; found, 1623.9267.

Synthesis of MeOTCz-DPyM. A procedure similar to that used for ***t*BuTCz-DPyM** was followed but using MeOTCz instead of *t*BuTCz to afford the compound **MeOTCz-DPyM** as a yellow solid with a yield of 56%. ^{1}H NMR (600 MHz, $CDCl_3$) δ 9.35 (d, J = 1.8 Hz, 2H), 8.61 (dd, J = 8.4, 1.8 Hz, 2H), 8.31 (d, J = 9.0 Hz, 4H), 8.26 (d, J = 1.8 Hz, 4H), 8.06 (d, J = 8.4 Hz, 2H), 7.70 (dd, J = 8.4, 1.8 Hz, 4H), 7.58 (d, J = 2.4 Hz, 8H), 7.33 (d, J = 9.0 Hz, 8H), 7.04 (dd, J = 9.0, 2.4 Hz, 8H), 3.95 (s, 24H). ^{13}C NMR (150 MHz, $CDCl_3$) δ 190.57, 154.67, 154.00, 151.49, 140.09, 138.29, 136.94, 132.79, 129.66, 126.37, 125.82, 123.49, 119.12, 117.66, 115.23, 113.42, 110.50, 102.99, 56.12. HRMS (APCI) m/z: $[M + H]^+$ calcd for $C_{91}H_{67}N_8O_9^+$, 1415.5026; found, 1415.5074.

OLED device fabrication and characterization. ITO patterned glass substrates (size 12 mm × 8 mm) were cleaned in an ultrasonic bath using acetone, isopropyl alcohol, and DI water for 15 min, respectively. After UV-ozone treatment for 3 min, a 40-nm-thick PEDOT:PSS layer was spin coated onto the ITO substrate, which was then heated at 150 °C for 15 min. Then, a 5-nm-thick PVK interlayer was spin coated on top of the PEDOT:PSS layer under nitrogen and annealed at 110 °C for 10 min. Subsequently, an emissive layer of the TADF dendrimer was spin coated from a chlorobenzene solution and annealed at 100 °C for 5 min. Finally, TPBI (40 nm), Yb (5 nm) and silver (120 nm) cathodes were deposited *via* thermal evaporation under vacuum conditions (1×10^{-7} torr). Characterization of the device performance was measured using a Keithley 2400 meter with a BM-7AS luminance colorimeter in an F-star optical measurement system. The EL spectra and CIE coordinates were recorded using a PR-788 photometer.

Author contributions

Cheng Zhang: methodology, data curation, and writing – review and editing. Hao Yan: OLED device fabrication and characterization and writing – review and editing. Yuting He: conceptualization, investigation, and writing – original draft. Yongshuai Chai: software, data curation, and validation. Deyun Zhou: project administration, supervision, and writing – review and editing.

Conflicts of interest

There are no conflicts to declare.

Acknowledgements

This work was supported by the Natural Science Basic Research Plan in Shaanxi Province of China (Program No. 2021JQ-664), and the Natural Science Foundation of Shaanxi Provincial Department of Education (Program No. 19JK0379).

Notes and references

1 Y. W. Xu, P. Xu, D. H. Hu and Y. G. Ma, Recent progress in hot exciton materials for organic light-emitting diodes, *Chem. Soc. Rev.*, 2021, **50**, 1030–1069.
2 X. C. Fan, K. Wang, Y. Z. Shi, J. X. Chen, F. Huang, H. Wang, Y. N. Hu, Y. Tsuchiya, X. M. Ou, J. Yu, C. Adachi and X. H. Zhang, Managing intersegmental charge-transfer and multiple resonance alignments of D_3-A typed TADF emitters for red OLEDs with improved efficiency and color purity, *Adv. Opt. Mater.*, 2021, **10**, 2101789.
3 C. Wu, C. S. Shi, Y. Y. Zheng, J. Y. Zhang, Y. F. Wang, N. Sun, Q. Wang and Z. H. Lu, Multifunctional luminophores with dual emitting cores: TADF emitters with AIE properties for efficient solution- and evaporation-processed doped and non-doped OLEDs, *Chem. Eng. J.*, 2022, **431**, 133249.
4 B. Li, Z. Yang, W. Q. Gong, X. H. Chen, D. W. Bruce, S. Y. Wang, H. L. Ma, Y. Liu, W. G. Zhu, Z. G. Chi and Y. F. Wang, Intramolecular through-space charge transfer based TADF-active multifunctional emitters for high efficiency solution-processed OLED, *Adv. Opt. Mater.*, 2021, **9**, 2100180.
5 J. N. Sun, J. Zhang, Q. Q. Liang, Y. Wei, C. B. Duan, C. M. Han and H. Xu, Charge-transfer exciton manipulation based on hydrogen bond for efficient white thermally activated delayed fluorescence, *Adv. Funct. Mater.*, 2020, **30**, 1908568.
6 Y. Liu, X. Xiao, Y. Ran, Z. Y. Bin and J. S. You, Molecular design of thermally activated delayed fluorescent emitters for narrowband orange–red OLEDs boosted by a cyano-functionalization strategy, *Chem. Sci.*, 2021, **12**, 9408–9412.
7 F. T. Liu, Z. Cheng, L. Wan, Z. J. Feng, H. Liu, H. X. Jin, L. Gao, P. Lu and W. S. Yang, Highly efficient multi-resonance thermally activated delayed fluorescence material with a narrow full width at half-maximum of 0.14 eV, *Small*, 2021, **18**, 2106462.
8 M. L. Yang, S. Shikita, H. Min, I. S. Park, H. Shibata, N. Amanokura and T. Yasuda, Wide-range color tuning of narrowband emission in multi-resonance organoboron

delayed fluorescence materials through rational imine/amine functionalization, *Angew. Chem., Int. Ed.*, 2021, **60**, 23142–23147.

9 Y. Zou, S. L. Gong, G. H. Xie and C. L. Yang, Design strategy for solution-processable thermally activated delayed fluorescence emitters and their applications in organic light-emitting diodes, *Adv. Opt. Mater.*, 2018, **6**, 1800568.

10 S. Y. Lee, T. Yasuda, H. Komiyama, J. Lee and C. Adachi, Thermally activated delayed fluorescence polymers for efficient solution-processed organic light-emitting diodes, *Adv. Mater.*, 2016, **28**, 4019–4024.

11 Y. K. Yang, S. M. Wang, Y. H. Zhu, Y. J. Wang, H. M. Zhan and Y. X. Cheng, Thermally activated delayed fluorescence conjugated polymers with backbone-donor/pendant-acceptor architecture for nondoped OLEDs with high external quantum efficiency and low roll-off, *Adv. Funct. Mater.*, 2018, **28**, 1706916.

12 C. S. Li, Y. W. Xu, Y. C. Liu, Z. J. Ren, Y. G. Ma and S. K. Yan, Highly efficient white-emitting thermally activated delayed fluorescence polymers: Synthesis, non-doped white OLEDs and electroluminescent mechanism, *Nano Energy*, 2019, **65**, 104057.

13 Y. Z. Shi, H. Wu, K. Wang, J. Yu, X. M. Ou and X. H. Zhang, Recent progress in thermally activated delayed fluorescence emitters for nondoped organic light-emitting diodes, *Chem. Sci.*, 2022, **13**, 3625–3651.

14 C. Zhang, H. Zeng, Q. Y. Huang, Y. Wang, Y. S. Chai, Y. Huang, S. L. Zhao and Z. Y. Lu, High-performance red electrophosphorescent devices based on all-solution-processed hydrogen-bonded supramolecular material, *J. Mater. Chem. C*, 2018, **6**, 4095–4105.

15 C. Zhang, Y. Wang, Q. Y. Huang, J. Zhou, Y. Huang, S. L. Zhao and Z. Y. Lu, A novel H-bonding self-assembly heteromeric molecular duplex bearing host and guest energy transfer units as high-performance electroluminescent material, *Dyes Pigm.*, 2018, **149**, 755–763.

16 Y. T. He, D. Y. Zhou, C. Zhang and H. Yan, Yongshuai Chai, Orange-red and saturated red thermally activated delayed fluorescent dendrimers for non-doped solution-processed OLEDs, *Dyes Pigm.*, 2022, **203**, 110385.

17 X. Yin, Y. He, X. Wang, Z. X. Wu, E. B. Pang, J. Xu and J. A. Wang, Recent advances in thermally activated delayed fluorescent polymer-molecular designing strategies, *Front. Chem.*, 2020, **8**, 725.

18 Q. Xue and G. H. Xie, Thermally activated delayed fluorescence beyond through-bond charge transfer for high-performance OLEDs, *Adv. Opt. Mater.*, 2021, **9**, 2002204.

19 T. C. Jiang, Y. C. Liu, Z. J. Ren and S. K. Yan, The design, synthesis and performance of thermally activated delayed fluorescence macromolecules, *Polym. Chem.*, 2020, **11**, 1555–1571.

20 F. M. Xie, J. X. Zhou, Y. Q. Li and J. X. Tang, Effects of the relative position and number of donors and acceptors on the properties of TADF materials, *J. Mater. Chem. C*, 2020, **8**, 9476–9494.

21 S. K. Jeon, H. L. Lee, K. S. Yook and J. Y. Lee, Recent progress of the lifetime of organic light-Emitting diodes based on thermally activated delayed fluorescent material, *Adv. Mater.*, 2019, **31**, 34.

22 Y. Zou, S. L. Gong, G. H. Xie and C. L. Yang, Design strategy for solution-processable thermally activated delayed fluorescence emitters and their applications in organic light-emitting diodes, *Adv. Opt. Mater.*, 2018, **6**, 1800568.

23 M. Godumala, S. Choi, M. J. Cho and D. H. Choi, Recent breakthroughs in thermally activated delayed fluorescence organic light emitting diodes containing non-doped emitting layers, *J. Mater. Chem. C*, 2019, **7**, 2172–2198.

24 X. X. Ban, W. Jiang, K. Y. Sun, B. P. Lin and Y. M. Sun, Self-host blue dendrimer comprised of thermally activated delayed fluorescence core and bipolar dendrons for efficient solution-processable nondoped electroluminescence, *ACS Appl. Mater. Interfaces*, 2017, **9**, 7339–7346.

25 C. S. Li, Z. J. Ren, X. L. Sun, H. H. Li and S. K. Yan, Deep-blue thermally activated delayed fluorescence polymers for nondoped solution-processed organic light-emitting diodes, *Macromolecules*, 2019, **52**, 2296–2303.

26 C. S. Li, A. K. Harrison, Y. C. Liu, Z. N. Zhao, C. Zeng, F. B. Dias, Z. J. Ren, S. Yan and M. R. Bryce, Asymmetrical-dendronized TADF emitters for efficient non-doped solution-processed OLEDs by eliminating degenerate excited states and creating solely thermal equilibrium routes, *Angew. Chem., Int. Ed.*, 2022, **61**, e202115140.

27 P. S. Ngo, M. K. Hung, K. W. Tsai, S. Sharma and S. A. Chen, Highly efficient solution-processed thermally activated delayed fluorescence bluish-green and hybrid white organic light-emitting diodes using novel bipolar host materials, *ACS Appl. Mater. Interfaces*, 2019, **11**, 45939–45948.

28 J. H. Lee, C. H. Chen, P. H. Lee, H. Y. Lin, M. Y. Leung, T. L. Chiu and C. F. Lin, Blue organic light-emitting diodes: current status, challenges, and future outlook, *J. Mater. Chem. C*, 2019, **7**, 5874–5888.

29 B. H. Zhang and Y. X. Cheng, Recent advances in conjugated TADF polymer featuring in backbone-donor/pendant-acceptor structure: material and device perspectives, *Chem. Rec.*, 2019, **19**, 1624–1643.

30 C. S. Li, R. S. Nobuyasu, Y. K. Wang, F. B. Dias, Z. J. Ren, M. R. Bryce and S. K. Yan, Solution-processable thermally activated delayed fluorescence white OLEDs based on dual-emission polymers with tunable emission colors and aggregation-enhanced emission properties, *Adv. Opt. Mater.*, 2017, **5**, 1700435.

31 Y. Zou, S. L. Gong, G. H. Xie and C. L. Yang, Design strategy for solution-processable thermally activated delayed fluorescence emitters and their applications in organic light-emitting diodes, *Adv. Opt. Mater.*, 2018, **6**, 1800568.

32 C. Yin, D. D. Zhang and L. Duan, A perspective on blue TADF materials based on carbazole-benzonitrile derivatives for efficient and stable OLEDs, *Appl. Phys. Lett.*, 2020, **116**, 120503.

33 X. J. Zheng, R. J. Huang, C. Zhong, G. H. Xie, W. M. Ning, M. L. Huang, F. Ni, F. B. Dias and C. L. Yang, Achieving 21% external quantum efficiency for nondoped solution-processed sky-blue thermally activated delayed fluorescence OLEDs by

means of multi-(donor/acceptor) emitter with through-space/-bond charge transfer, *Adv. Sci.*, 2020, **7**, 1902087.

34 J. Hwang, H. Kang, J. E. Jeong, H. Y. Woo, M. J. Cho, S. Park and D. H. Choi, Donor engineered deep-blue emitters for tuning luminescence mechanism in solution-processed OLEDs, *Chem. Eng. J.*, 2021, **416**, 129185.

35 B. Wex and B. R. Kaafarani, Perspective on carbazole-based organic compounds as emitters and hosts in TADF applications, *J. Mater. Chem. C*, 2017, **5**, 8622–8653.

36 K. Matsuoka, K. Albrecht, A. Nakayama, K. Yamamoto and K. Fujita, Highly efficient thermally activated delayed fluorescence organic light-emitting diodes with fully solution-processed organic multilayered architecture: impact of terminal substitution on carbazole-benzophenone dendrimer and interfacial engineering, *ACS Appl. Mater. Interfaces*, 2018, **10**, 33343–33352.

37 J. J. Luo, S. L. Gong, Y. Gu, T. H. Chen, Y. F. Li, C. Zhong, G. H. Xie and C. L. Yang, Multi-carbazole encapsulation as a simple strategy for the construction of solution-processed, non-doped thermally activated delayed fluorescence emitters, *J. Mater. Chem. C*, 2016, **4**, 2442–2446.

38 K. Albrecht, E. Matsuoka, D. Yokoyama, Y. Sakai, A. Nakayama, K. Fujita and K. Yamamoto, Thermally activated delayed fluorescence OLEDs with fully solution processed organic layers exhibiting nearly 10% external quantum efficiency, *Chem. Commun.*, 2017, **53**, 2439–2442.

39 Y. F. Li, G. H. Xie, S. L. Gong, K. L. Wu and C. L. Yang, Dendronized delayed fluorescence emitters for non-doped, solution-processed organic light-emitting diodes with high efficiency and low efficiency roll-off simultaneously: two parallel emissive channels, *Chem. Sci.*, 2016, **7**, 5441–5447.

40 B. Huang, X. X. Ban, K. Y. Sun, Z. M. Ma, Y. N. Mei, W. Jiang, B. P. Lin and Y. M. Sun, Thermally activated delayed fluorescence materials based on benzophenone derivative as emitter for efficient solution-processed non-doped green OLED, *Dyes Pigm.*, 2016, **133**, 380–386.

41 P. Rajamalli, D. Y. Chen, W. B. Li, I. D. W. Samuel, B. C. David, M. Z. S. Alexandra and E. Zysman-Colman, Enhanced thermally activated delayed fluorescence through bridge modification in sulfone-based emitters employed in deep blue organic light-emitting diodes, *J. Mater. Chem. C*, 2019, **7**, 6664–6671.

42 H. Uoyama, K. Goushi, K. Shizu, H. Nomura and C. Adachi, Highly efficient organic light-emitting diodes from delayed fluorescence, *Nature*, 2012, **492**, 234–238.

43 S. Hirata, Y. Sakai, K. Masui, H. Tanaka, S. Y. Lee, H. Nomura, N. Nakamura, M. Yasumatsu, H. Nakanotani, Q. S. Zhang, K. Shizu, H. Miyazaki and C. Adachi, Highly efficient blue electroluminescence based on thermally activated delayed fluorescence, *Nat. Mater.*, 2015, **14**, 330–336.

44 K. C. Pan, S. W. Li, Y. Y. Ho, Y. J. shiu, W. L. Tsai, M. Jiao, W. K. Lee, C. C. Wu, C. L. Chung, T. Chatterjee, Y. S. Li, K. T. Wong, H. C. Hu, C. C. Chen and M.-T. Lee, Efficient and tunable thermally activated delayed fluorescence emitters having orientation-adjustable CN-substituted pyridine and pyrimidine acceptor units, *Adv. Funct. Mater.*, 2016, **26**, 7560–7571.

45 X. Zeng, K. C. Pan, W. K. Lee, S. L. Gong, F. Ni, X. Xiao, W. X. Zeng, Y. P. Xiang, L. S. Zhan, Y. Zhang, C. C. Wu and C. L. Yang, High-efficiency pure blue thermally activated delayed fluorescence emitters with a preferentially horizontal emitting dipole orientation via a spiro-linked double D-A molecular architecture, *J. Mater. Chem. C*, 2019, **7**, 10851–10859.

46 S. Y. Hsieh, Y. Tang, S. Crotti, E. A. Stone and S. J. Miller, Catalytic enantioselective pyridine N-oxidation, *J. Am. Chem. Soc.*, 2019, **141**, 18624–18629.